ACS APPLIED MATERIALS & INTERFACES

Research Article

www.acsami.org

Generation and Properties of Antibacterial Coatings Based on Electrostatic Attachment of Silver Nanoparticles to Protein-Coated Polypropylene Fibers

Kiran K. Goli,[†] Nimish Gera,[‡] Xiaomeng Liu,[§] Balaji M. Rao,[‡] Orlando J. Rojas,[‡,§,∥] and Jan Genzer*[,‡]

[†]Department of Materials Science & Engineering, North Carolina State University, Raleigh, North Carolina 27695-7907, United States

[‡]Department of Chemical & Bimolecular Engineering, North Carolina State University, Raleigh, North Carolina 27695-7905, United States

[§]Department of Forest Biomaterials, North Carolina State University, Raleigh, North Carolina 27695-8204, United States

[∥]Department of Forest Products Technology, Aalto University, FI-00076 Aalto, Espoo, Finland

Supporting Information

ABSTRACT: We present a simple method for attaching silver nanoparticles to polypropylene (PP) fibers in a two-step process to impart antibacterial properties. Specifically, PP fibers are pretreated by the adsorption from an aqueous solution of heat-denatured lysozyme (LYS) followed by LYS cross-linking using glutaraldehyde and sodium borohydride. At neutral pH, the surface of the adsorbed LYS layer is enriched with numerous positive charges. Silver nanoparticles (AgNPs) capped with trisodium citrate are subsequently deposited onto the protein-coated PP. Nanoparticle binding is mediated by electrostatic interactions between the positively charged LYS layer and the negatively charged AgNPs. The density of AgNPs deposited on PP depends on the amount of protein adsorbed on the surface. UV−vis spectroscopy, transmission electron microscopy, Fourier transform infrared spectroscopy, and scanning electron microscopy are employed to follow all preparation steps and to characterize the resulting functional surfaces. The antibacterial activity of the modified surfaces is tested against gram negative bacteria *Escherichia coli* (*E. coli*). Overall, our results show that PP surfaces coated with AgNPs exhibit excellent antibacterial activity with 100% removal efficiency.

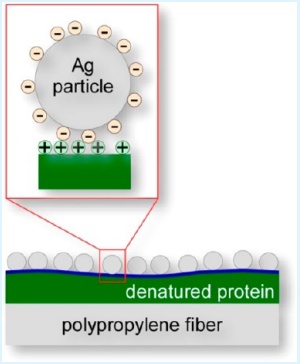

KEYWORDS: *antibacterial, polypropylene, protein adsorption, nanoparticle, functional coating*

1. INTRODUCTION

Surfaces with antibacterial properties are highly desired in applications that require a protective barrier against infection. The extensive use of synthetic polymeric materials in health and biomedical, food, textile, packaging, and personal hygiene industries thus demands incorporation of biocidal compounds.[1] This is because most polymers employed in the aforementioned fields are prone to bacterial adhesion, leading to cell growth and colonization, resulting potentially in severe infections and disease transmission.[1,2]

The growth of harmful microorganisms on surfaces can be delayed, reduced, or even inhibited by the incorporation of biocidal agents into the bulk polymeric materials.[3,4] Coatings based on slow release of these biocides, i.e., heavy metals, antibiotics, small biocide molecules, halogen species, and nitric oxide, render surfaces with effective antimicrobial properties.[1] An alternative strategy is to immobilize cationic polymers with quaternary ammonium groups onto various substrates.[5] Since the action of quaternary ammonium compounds against microbes is limited to specific targets, the efficiency of these materials decreases with prolonged exposures.[6−8] Several studies confirmed that silver nanoparticles (AgNPs) possess excellent antimicrobial activity against a broad spectrum of microbes.[9] In addition, AgNPs are less toxic to human cells as compared to other metals.[10] Possible targets for silver inside the microbial cells are numerous, and hence, the development/evolution of its resistance against silver compounds is limited.[7,11] Owing to its small size, i.e., large surface area, AgNPs bind efficiently to the microorganisms and provide enhanced antimicrobial action.[12] AgNPs interact with sulfur and phosphorus compounds of membrane proteins affecting cell morphology and structure, causing its death. In addition, AgNPs bind to DNA in the interior of the cell, resulting in disruption of its replication ability as well as inactivation of cellular proteins.[1,9,13,14] However, attaching these antibacterial agents to the surfaces of polymeric materials, especially in the case of hydrophobic surfaces, is a very challenging task. The increasing use of polypropylene (PP) nonwovens in medical, institutional, and hygienic applications demands methods that would endow them with antimicrobial properties. PP has

Received: March 31, 2013
Accepted: May 15, 2013
Published: May 15, 2013

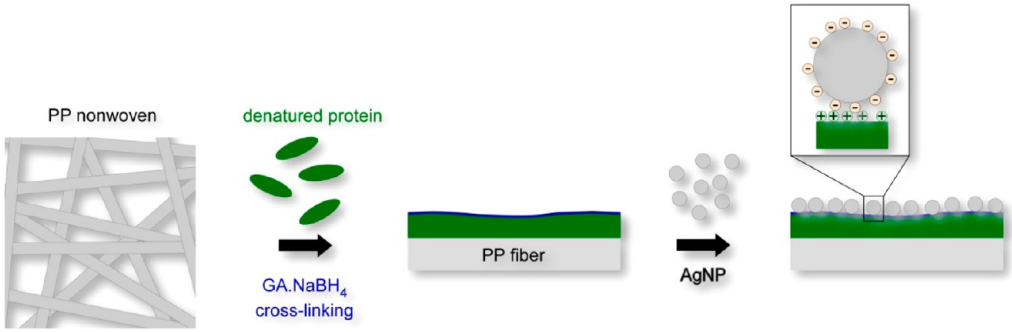

Figure 1. Schematic illustration of the steps leading to the deposition of silver nanoparticles onto PP fiber primed with denatured proteins.

become a material of choice for numerous applications due to its superior bulk properties including chemical inertness, mechanical characteristics, low density, and low cost.[15,16] However, low surface energy and lack of functional groups restrict the development of desirable coatings on PP surfaces without aggressive preactivation treatments. Flame,[17] corona discharge,[3] plasma,[18] UV light,[19] and electron beam[20] treatments are the most common approaches employed to activate such surfaces and to introduce desired chemical groups on PP and other polymer surfaces.[2,16,21] These surface modification processes convert such inexpensive materials into highly valuable products featuring functional coatings.[16] Abdou et al.[22] deposited chitosan onto PP nonwovens preactivated with plasma irradiation and demonstrated effective antimicrobial activity. Huang et al.[2] grafted a ternary polymer brush, poly(2-dimethylaminoethyl methacrylate) (PDMAEMA), onto PP surfaces via surface-initiated atom transfer radical polymerization (ATRP), providing strong antibacterial activity against *E. coli*. Yao et al.[5] reported on grafting of block copolymer brushes of poly(ethylene glycol) monomethacrylate (PEGMA) and DMAEMA (PEGMA-*b*-PDMAEMA) onto PP hollow fiber membranes via surface-initiated ATRP. The polymer grafted surfaces exhibited permanent antibacterial activity. However, the disadvantages of methods that require physical modification is that they damage the PP surface due to etching.[15] This physical modification approach is particularly challenging in the case of finer fibers, since it can seriously compromise their mechanical properties.

We have recently demonstrated a convenient method to functionalize hydrophobic and hydrophilic surfaces through the adsorption of denatured proteins.[23−26] The protein coating provides the surface with hydrophilic functionalities, which can be further utilized to introduce new surface chemistries and physical properties. In addition, our surface modification process is less severe, aqueous-based, fast, relatively robust, and facile.[24] In this paper, we use the protein surface modification technique through the physical adsorption of denatured lysozyme (LYS) proteins on PP nonwovens. The amino acid functional groups present on the periphery of the adsorbed protein layer serve as anchoring points for the attachment of AgNPs. Specifically, the amount of protein adsorbed on PP nonwoven surfaces is altered by varying the experimental conditions during protein deposition, i.e., the pH and concentration of proteins in the adsorption solution. Subsequently, AgNPs are deposited on the preadsorbed protein layers, endowing PP nonwovens with efficient antibacterial activity, as evaluated by a biocidal test against *Escherichia coli (E. coli)*.

2. MATERIALS AND METHODS

Deionized water (DIW) (resistivity >16 MΩ cm) was produced using a Millipore water purification system. PP nonwovens were obtained from the Nonwovens Institute pilot facilities at NC State University and were cleaned with isopropanol prior to use. Lysozyme (from chicken egg white, M_n = 14.3 kDa, pI = 11.3), glutaraldehyde (GA), silver nitrate ($AgNO_3$), sodium borohydride ($NaBH_4$), and sodium citrate tribasic dihydrate (TSC) were purchased from Sigma-Aldrich and were used as received. D/E (Dey/Engley) neutralizing broth with Tween surfactant was purchased from Neogen Corporation.

Preparation of Silver Nanoparticles. Silver nanoparticles were prepared by chemically reducing $AgNO_3$ with $NaBH_4$ in the presence of TSC according to procedures described elsewhere.[27,28] Briefly, aqueous solutions of $AgNO_3$ and TSC in equal molarities were mixed together under vigorous stirring for 5 min. To this solution, $NaBH_4$ predissolved in water was added rapidly in one batch at room temperature. The stirring was stopped after 1 h. Upon the addition of $NaBH_4$, the transparent solution was converted to characteristic pale to deep yellow color depending upon the concentration of $AgNO_3$, demonstrating the formation of AgNPs. Jana and co-workers[28] synthesized AgNPs at the silver nitrate concentrations of 0.25 mM, producing nanoparticles having diameters between 3 and 5 nm. In this work, AgNPs were prepared at four different concentrations of $AgNO_3$, 0.25, 0.5, 1, and 2 mM, while keeping the final molar ratios of $AgNO_3$, TSC, and $NaBH_4$ constant. Sample A (Ag(0.25)NP, x_{Ag} = 0.25 mM) was prepared to obtain $AgNO_3$, TSC, and $NaBH_4$ final concentrations of 0.25, 0.25, and 0.3 mM, respectively. Sample B (Ag(0.5)NP, x_{Ag} = 0.5 mM) was prepared to obtain $AgNO_3$, TSC, and $NaBH_4$ final concentrations of 0.5, 0.5, and 0.6 mM, respectively. Sample C (Ag(1.0)NP, x_{Ag} = 1.0 mM) was prepared to obtain $AgNO_3$, TSC, and $NaBH_4$ final concentrations of 1.0, 1.0, and 1.2 mM, respectively. Sample D (Ag(2.0)NP, x_{Ag} = 2.0 mM) was prepared to obtain $AgNO_3$, TSC, and $NaBH_4$ final concentrations of 2.0, 2.0, and 2.4 mM, respectively.

Adsorption of Denatured Protein Solutions on PP Nonwoven Surfaces. Denatured protein coatings were prepared on PP nonwoven sheets as described in our previous work.[24] Briefly, LYS solutions at required concentrations (i.e., 0.01 and 1 mg/mL) were prepared in PBS buffer. The solution pH was adjusted to desired levels of 7.4 and 10. The proteins were allowed to solubilize for 6 h followed by heating for 3 min in a preheated oven at 85 °C before incubating PP nonwoven substrates for 15 min. The stability of the protein coatings on PP nonwoven sheets was improved by cross-linking with GA and $NaBH_4$.

Deposition of AgNPs on PP Nonwoven Surfaces. Unmodified PP used as control and LYS-coated PP fibers with different amounts of proteins on their surface were incubated overnight at room temperature in AgNP colloidal dispersion with a high molar concentration of nanoparticles (Ag(2.0)NP). This process resulted in adsorption of AgNPs on the protein-pretreated PP surfaces. A schematic illustrating the deposition of AgNPs on protein-coated PP nonwoven surfaces is shown in Figure 1. The resultant fibers were rinsed copiously with DI water followed by sonication in PBS buffer

for 2 min to remove loosely bound AgNPs. The samples were then characterized with UV−vis, SEM imaging, and antibacterial activity.

Antibacterial Activities of PP Nonwovens with Adsorbed Ag(2.0)NPs. *Test Method a.* The antibacterial properties of control PP, LYS-coated PP (PP-LYS), and Ag(2.0)NP-treated PP-LYS (PP-LYS-Ag(2.0)NP) fibers were analyzed against *E. coli* DH5-α using an ASTM standard: the E2180-07 standard test method for determining the activity of incorporated antimicrobial agents in polymeric or hydrophobic materials. Luria broth (LB) agar slurry (1 mL) containing ~5 × 10^6 cells/mL was placed on a 3.0 × 3.0 cm^2 test specimen followed by spreading with a cotton swab, forming a thin film. The agar slurry on the test specimens were allowed to gel at room temperature followed by incubation at 37 °C for 18 h. After incubation, the samples were subjected to vigorous mechanical vortexing for 3 min in a neutralizing broth to release the agar slurry from the sample. The resultant suspension containing cells was then diluted with LB medium to the desired concentration followed by plating them on LB agar growth plates. The agar plates were incubated at 37 °C for 18 h, and the number of viable cells was determined as colony forming units (CFU). After incubation, each surviving cell developed into a distinct colony, and colony counts were used to determine the bacterial activity. The antibacterial effectiveness was calculated as the bacterial removal percentage following eq 1

$$\text{Bacterial killing percentage} = \frac{D_{\text{control}}N_{\text{control}} - D_{\text{sample}}N_{\text{sample}}}{D_{\text{control}}N_{\text{control}}} 100\% \quad (1)$$

where N_{control} and N_{sample} are the numbers of bacterial colonies counted on LB agar plates corresponding to control PP and treated PP nonwovens, respectively. D_{control} and D_{sample} are the dilution factors of control PP and treated PP nonwovens, respectively.

Test Method b. The antibacterial activity of the PP nonwoven surfaces before and after treatment with protein and Ag(2.0)NPs was also tested against *E. coli* using a slight modification of AATCC test method 147-1998 "Antibacterial activity assessment of textile materials" by the parallel streak method. The test specimen (nonwoven mat) with dimensions of 2 × 2 cm^2 was placed at the center of a standard Petri dish. Agar slurry (5 mL) containing ~1 × 10^5 CFU/mL of *E. coli* was dispensed into the Petri dish with nonwoven mat, and the slurry was spread, forming a uniform thin film. The test specimen was in an intimate contact with the bacterial agar slurry. The agar slurry was allowed to solidify at room temperature. The plates were then incubated at 37 °C for 18 h. The resultant plates were then examined visually for growth of bacteria in the area surrounding the nonwoven mat. The formation of a clear zone around the fabric (i.e., inhibition zone) was measured, and the results were reported as the average width of the zone of inhibition (in mm) extending beyond the edge of the nonwoven mat. A Nikon Eclipse TS 100 Microscope with 4× magnification was used to image the nonwoven mat near the edge and the inhibition zone.

Ultraviolet−Visible (UV−vis) Analysis. A Jasco V-550 UV−vis spectrophotometer was used to analyze the synthesized nanoparticles. The analysis was conducted by collecting the spectrum over a wavelength range of 300−700 nm with a resolution of 0.5 nm. Ag(2.0)NP treated PP nonwoven sheets were characterized by carrying UV−vis analysis in the 320−700 nm wavelength range. Prior to the measurements, nanoparticle solutions were diluted 40-fold with deionized water.

Transmission Electron Microscopy (TEM). AgNPs prepared at different concentrations of $AgNO_3$ were characterized using JEOL 2010F-FasTEM at an operating voltage of 200 kV. The samples were prepared by placing a drop of the nanoparticle colloid dispersion on a carbon-coated copper grid. The drop was allowed to dry overnight in air. The shape and size distribution of the nanoparticles were characterized by TEM. The histograms prepared by measuring the sizes of nanoparticles from TEM images reveal information about the size distribution of nanoparticles. Statistical analysis was performed by one-way ANOVA to determine the differences in nanoparticle sizes prepared at different concentrations of silver nitrate. *P* values less than 0.05 were considered to be statistically significant.

Zeta Potential Measurements. The zeta potential of silver nanoparticle suspensions was measured using a Zetasizer Nano-ZS instrument (Malvern Instruments Ltd., UK). We observed that the aqueous suspensions of the nanoparticles were stable if the zeta potential was greater than ca. +30 mV or less than −30 mV. The state of aggregation was assessed by particle sizing in the respective dispersion and TEM imaging.

Scanning Electron Microscopy (SEM). The presence of nanoparticles and their coverage after Ag(2.0)NP deposition on PP nonwoven surfaces were examined under a Hitachi S-4700 SEM operating at 20 kV in high vacuum mode after sputter-coating with a thin layer of gold−palladium metal.

Inductively Coupled Plasma (ICP). The content of silver on PP nonwovens after Ag(2.0)NP deposition was quantified by inductively coupled plasma-optical emission spectroscopy (ICP-OES) (Perkin-Elmer, Optima 2000 DV). Briefly, PP samples weighing to the nearest 0.0001 g were placed into 250 mL Teflon bottles. A 5 mL portion of 4:1 HCl:HNO_3 (Trace Metal grade) was added to each bottle/sample, loosely capped, and allowed to predigest overnight. Subsequently, the acid digestates were heated in a sand bath at ~95 °C for 2 h. Samples were removed from the sand bath and allowed to cool for ~30 min. A 1 mL portion of concentrated HCl was added to each sample, and they were refluxed again at ~95 °C for 1 h. After this time, the samples were cooled and filtered through a Whatman #41 filter paper, using 2% v/v HCl to rinse the filter repeatedly, and to bring each digestate to a final volume of 25 mL. The digestates were diluted 10-fold with 2% HCl, and analyzed at a wavelength of ~328 nm, against a multicalibration curve (Spex Certiprep ICP-MS grade standard solution) having an acid-matrix matched background to the sample digestates.

3. RESULTS AND DISCUSSION

3.1. Preparation of Silver Nanoparticles at Different Molar Concentrations. AgNPs were synthesized by chemical reduction of $AgNO_3$ with $NaBH_4$ in the presence of TSC as a capping agent. The presence of anionic TSC stabilizes the nanoparticles by electrostatic repulsion and prevents their aggregation.[27,28] UV−visible spectra of AgNPs prepared at different concentrations as detailed in the Materials and Methods section are shown in Figure 2. As the concentration

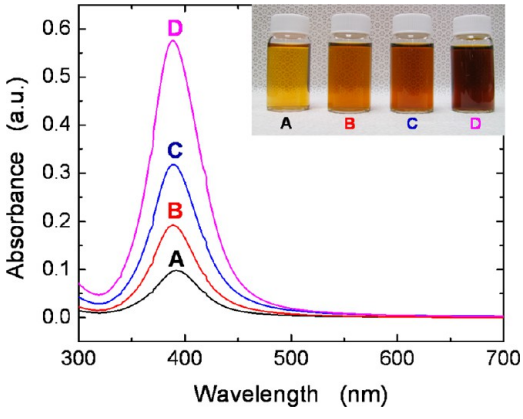

Figure 2. UV−visible spectra of silver nanoparticles prepared in aqueous solutions at four different molar concentrations of $AgNO_3$: (A) x_{Ag} = 0.25 mM, (B) x_{Ag} = 0.5 mM, (C) x_{Ag} = 1.0 mM, and (D) x_{Ag} = 2.0 mM. The inset shows the photographs of solutions containing AgNPs synthesized with different molar concentrations of $AgNO_3$ represented by (A) Ag(0.25)NP, (B) Ag(0.5)NP, (C) Ag(1.0)NP, and (D) Ag(2.0)NP. A variation in visible color can be observed with increasing molar concentrations of parts A−D.

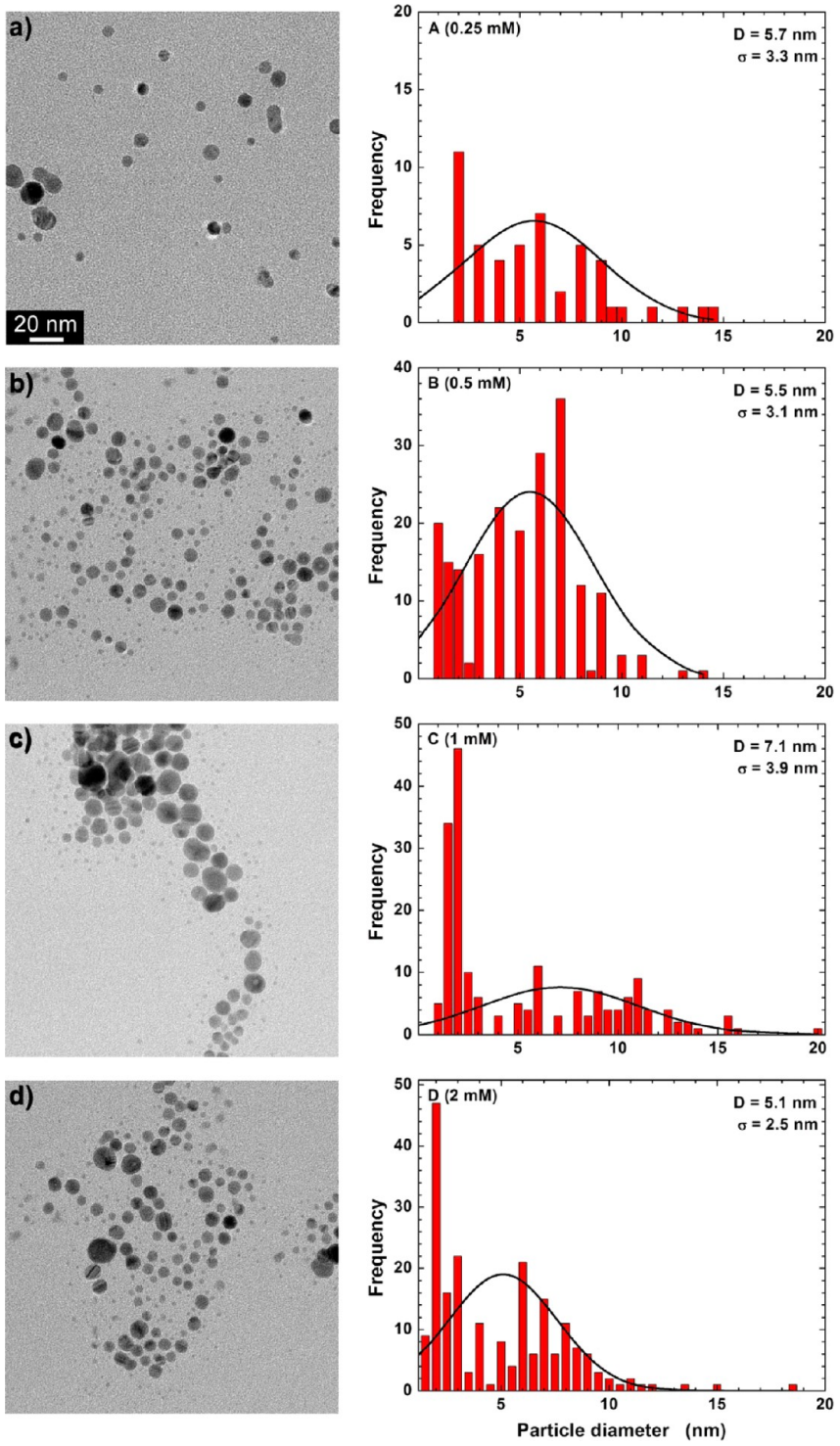

Figure 3. TEM images and size distribution histograms of AgNPs prepared from molar concentrations of $AgNO_3$: (a) Ag(0.25)NP; (b) Ag(0.5)NP; (c) Ag(1.0)NP; (d) Ag(2.0)NP.

of $AgNO_3$ in solution increases, the concentration of silver nanoparticles per unit volume increases accordingly. The photograph in the inset in Figure 2 documents clearly that the silver colloids are yellow in color at lower concentrations and turn into deep yellow/darker color with the increasing molar concentrations of the precursor. Particle size and size distribution of AgNPs in the colloids affect the position, shape, and symmetry of the surface plasmon absorption band of silver. The absorption peak observed at ~390 nm in Figure 2 corresponds to the typical surface plasmon resonance absorption of spherical AgNPs with sizes ranging between 3 and 20 nm.[29−31] An increase in the UV absorption peak intensity was observed with increasing concentration of $AgNO_3$, which might be attributed to the occurrence of two phenomena including a significant change in the nanoparticle size due to aggregation or increasing the number density of nanoparticles in solution. However, no obvious shift in the absorption maximum toward the larger wavelengths is evident

from the UV−vis spectra with increasing molar concentrations of silver precursor, suggesting that the increase in intensity might be the result of the latter phenomenon. Dong et al.[32] prepared AgNPs from $AgNO_3$ using different concentrations of TSC and $NaBH_4$. The authors demonstrated that the decrease in the intensity of surface plasmon resonance is attributed to the decreased amount of AgNPs in solution. TEM images of silver colloids prepared at different molar concentrations and the respective size distribution histograms are shown in Figure 3. The TEM images indicate that AgNPs prepared at different concentrations of $AgNO_3$ are nearly spherical in shape and exhibit similar sizes. The average size and size distribution of the AgNPs were determined by analyzing at least 150 nanoparticles except for Ag(0.25)NP. The number density of AgNPs observed on the TEM grid with x_{Ag} = 0.25 mM is smaller than that for other concentrations. The average particle size for silver nanoparticles is ~5 ± 4 nm; there is no noticeable change in the mean size with increasing molar concentrations of the reagents. The statistical analysis using one-way analysis of variance reveals that there are no significant differences between the average sizes of nanoparticles prepared at all concentrations with a confidence level of 95%. Owing to its strong reducing power, $NaBH_4$ reacts fast with $AgNO_3$ and forms small nanoparticles.[30,33] The total concentration of Ag ions reduced to Ag atoms was determined using a Ag ion-selective electrode (see the Supporting Information). Using the percent conversion of Ag ions to silver atoms, the molar concentration of AgNPs was calculated by assuming that the nanoparticles have a spherical shape with a mean diameter of 5 nm. The corresponding results are summarized in Table 1.

Table 1. Molar Concentrations of AgNPs with Different Initial Concentrations of Silver Nitrate

sample	% conversion of silver ions to silver atoms in nanoparticle dispersion	molar concentration of nanoparticles (M)
A (Ag(0.25)NP)	62.3	4.06×10^{-8}
B (Ag(0.5)NP)	89.1	1.16×10^{-7}
C (Ag(1.0)NP)	97.1	2.53×10^{-7}
D (Ag(2.0)NP)	98.4	5.22×10^{-7}

From the results, it is evident that the molar concentrations of nanoparticles obtained with x_{Ag} = 2 mM (Ag(2.0)NP) is 12 times greater than that of x_{Ag} = 0.25 mM (Ag(0.25)NP). This supports our earlier statement, namely, that increasing the concentration of $AgNO_3$ increases preferentially the number density of nanoparticles in the solution. Turkevich[34] prepared gold nanoparticle solutions at different concentrations and demonstrated that, when the initial concentration of solute is high, the formation of a large number of nuclei at the nucleation step is favored, generating more nanoparticles with smaller sizes and narrowed-down size distribution. Similar results are obtained in our work, where the concentration of nanoparticles in the solution increases with increasing initial concentrations of the precursor. In addition, though the mean size of nanoparticle is ~5 nm at all the concentrations, a large number of nanoparticles with sizes smaller than 5 nm is present for the case of Ag(1.0)NP and Ag(2.0)NP as compared to Ag(0.5)NP (cf. Figure 3). The zeta potential for the nanoparticles synthesized with x_{Ag} = 0.25 mM (Ag(0.25)NP) was ~ −29.3 ± 5 mV, in agreement with an earlier report of Cumberland et al.[35] who used a similar synthesis method. This confirms that the TSC and excess $NaBH_4$ present in the colloidal dispersion are adsorbed on the surface of the AgNPs, ensuring a stable and well-dispersed suspension resulting in a high stability of AgNPs. No significant differences in the zeta potentials were observed for nanoparticles obtained with increasing molar concentrations of precursor. AgNPs obtained with high molar concentrations (i.e., Ag(2.0)NP) were used in this work for adsorption on PP nonwoven substrates, as discussed in the next sections.

3.2. Deposition of Silver Nanoparticles on Protein-Coated PP Nonwoven Surfaces. In our previous work, we reported on the formation of stable denatured protein layers on hydrophobic surfaces featuring *n*-octadecyltrichlorosilane (ODTS) and PP nonwovens. Figure 4 shows a schematic of the method leading to adsorption of heat-denatured proteins on PP nonwovens. Specifically, heat-denatured LYS was adsorbed on flat ODTS-coated silica waters and PP nonwoven surfaces through nonspecific interactions. The amount of protein adsorbed (i.e., protein coverage) was varied by changing conditions implemented during protein adsorption including the concentration of protein in the solution, pH, and adsorption time. The following conditions provided LYS-modified ODTS substrates with variation in fractional protein coverage of 0.44 (PP-LYS(0.44)), 0.75 (PP-LYS(0.75)), and 1.1 (PP-LYS(1.1)): (a) 0.01 mg/mL LYS adsorbed at pH 7.4 and 85 °C for 15 min, (b) 0.01 mg/mL LYS adsorbed at pH 10 and 85 °C for 15 min, and (c) 1 mg/mL LYS adsorbed at pH 10 and 85 °C for 15 min.[24] Substrates with different amounts of adsorbed protein were used for the deposition of Ag(2.0)NP. The presence of protein on PP nonwoven surfaces was confirmed by IR spectroscopy shown in Figure 4. The characteristic amide I (C═O stretching) and amide II (C—N stretching and N—H bending) bands observed at wave numbers of 1700−1550 and 3420−3250 cm^{-1}, respectively, verify the protein immobilization on the PP surface.[36,37] The isoelectric point of LYS is ~11.3.[24] Thus, depending upon the pH of the solution, LYS carries net positive or negative charges, below or above its isoelectric point, respectively. Hence, LYS-adsorbed PP nonwovens exhibit cationic character at neutral pH. By taking advantage of these positive charges, negatively charged Ag(2.0)NPs were attached to the LYS-modified supports through electrostatic interactions (cf. Figure 1). Dipping PP nonwovens with varying fractional protein

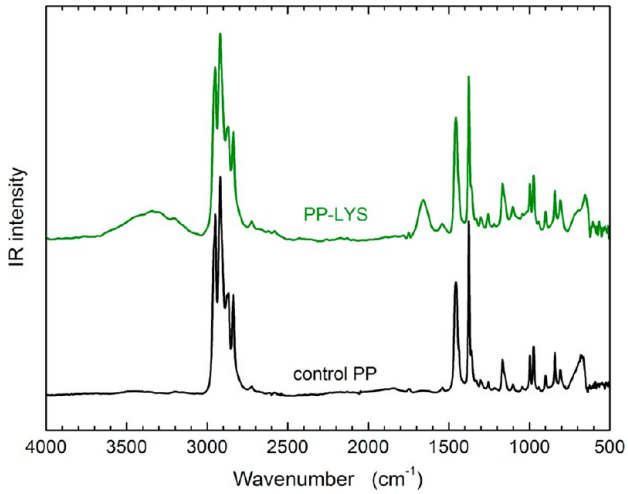

Figure 4. IR spectra of untreated PP (bottom) and PP modified with LYS (top).

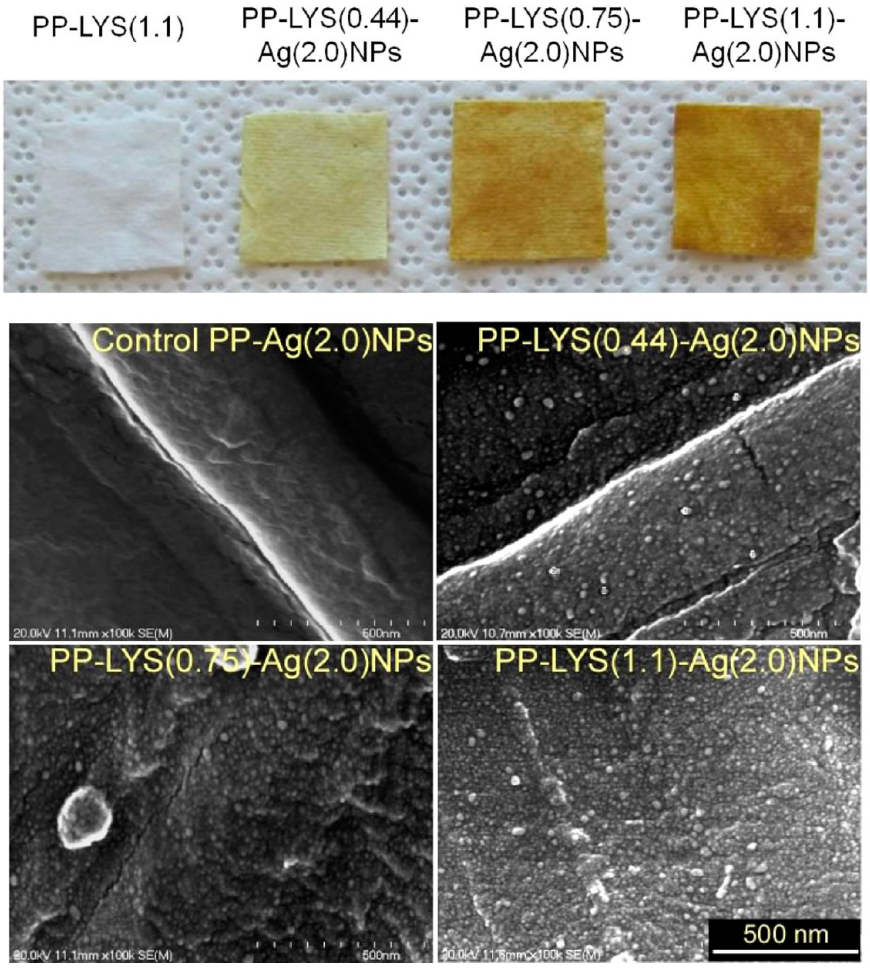

Figure 5. Control and protein modified PP nonwovens coated with silver nanoparticles. The sample dimensions are ~3 × 3 cm^2 (top). Respective SEM images of the corresponding PP nonwovens after treatment with silver nanoparticles (Ag(2.0)NP).

coverage in Ag(2.0)NP sols at pH 7.4 resulted in the deposition of silver nanoparticles. The nanoparticle adsorption was evident by a prominent color appearing over the fiber surfaces, as shown in Figure 5. Protein-precoated surfaces provided numerous accessible sites on the periphery of the protein layer that facilitated easy fixation of Ag(2.0)NP through electrostatic interactions. For instance, Mandal et al.[38] demonstrated the binding of cysteine to the surface of the silver particles via thiolate linkages of free thiol groups and colloidal silver. To some extent, we presume that the inherent affinity of these cysteine groups of protein also promoted the uptake of Ag(2.0)NP. The quantity of silver bound to PP nonwoven was determined by the inductively coupled plasma (ICP) method (cf. Figure 8). The results suggest that the concentration of Ag(2.0)NP increases with increasing protein coverage on the surfaces. SEM images of unmodified PP and LYS-modified PP nonwoven surfaces after the deposition of AgNPs are displayed in Figure 5. AgNPs were not observed on the surface of unmodified PP nonwoven after exposing to solutions containing Ag(2.0)NPs. In contrast, Ag(2.0)NPs are clearly visible on the surface of LYS-modified PP surfaces. These results support the conclusion that electrostatic interactions between the positive charges present at the top surface of the protein layer and the negatively charged AgNPs promote particle deposition. Figure 6 summarizes the UV−vis absorbance spectra of control (i.e., PP-LYS) and Ag(2.0)NP-

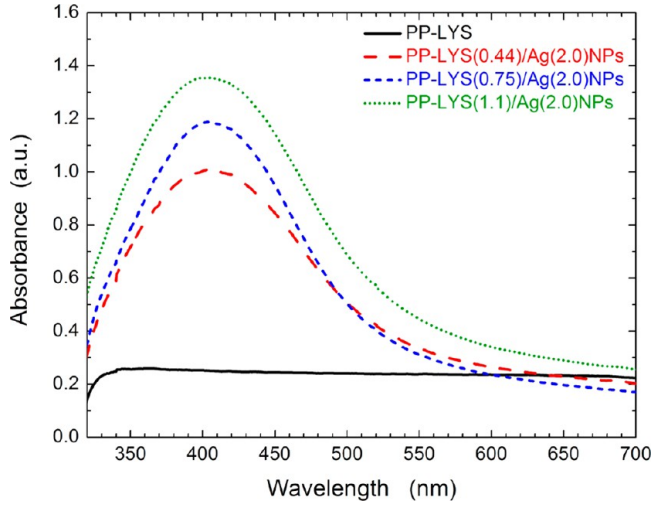

Figure 6. UV−visible absorbance spectra of PP-LYS (1.1) nonwoven (solid black) and PP-LYS coated with silver nanoparticles after using varying amounts of proteins: PP-LYS(0.44)/AgNPs (dashed red), PP-LYS(0.75)/AgNPs (short-dashed blue), and PP-LYS(1.1)/AgNPs (dotted green).

decorated nonwoven mats. The appearance of a characteristic surface plasmon resonance peak at ~404 nm after the deposition of nanoparticles on PP nonwoven substrates clearly

dx.doi.org/10.1021/am4011644 | ACS Appl. Mater. Interfaces 2013, 5, 5298−5306

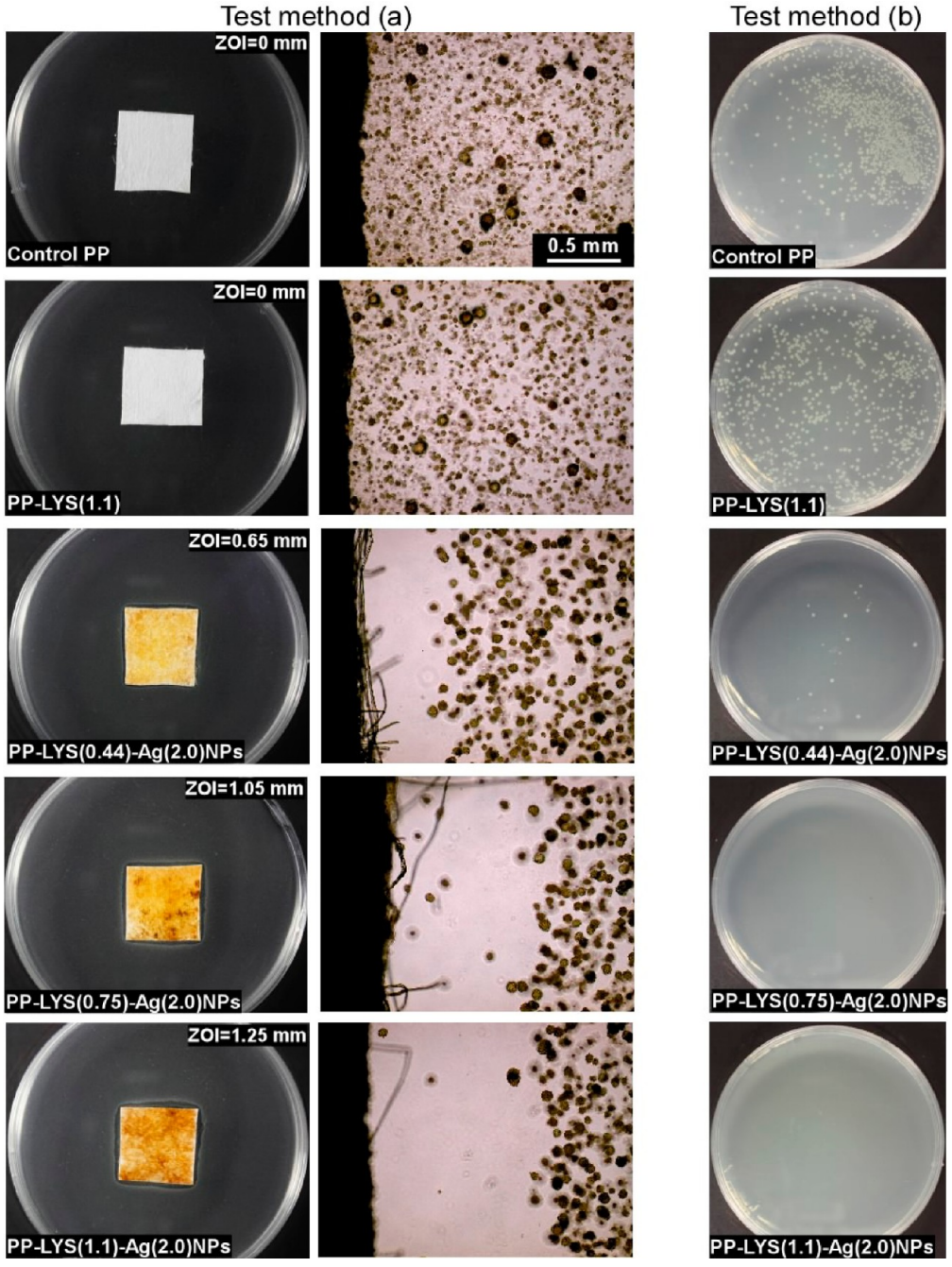

Figure 7. (Test method a) The antibacterial activity of control PP and silver nanoparticle treated PP nonwoven mats. The zone of inhibition (ZOI) can be observed around the silver nanoparticle treated mats and is shown at the top right corner of the plates. The sample dimensions are ~2 × 2 cm^2. The images at the bottom of the Petri dish show the corresponding enlarged optical microscopy images taken at the edge of the nonwoven mat (left column). (Test method b) LB plates corresponding to the *E. coli* suspension recovered from control and treated PP nonwovens. The colonies on the plates were counted, and the percent killing efficiency is reported in Table 2.

indicates the presence of AgNP. A shift in the surface plasmon peak toward larger wavelengths was noticed as compared to the surface plasmon peak (390 nm) of silver nanoparticles in solutions. This red shift might be attributed to either closer proximity of Ag(2.0)NPs on the nonwoven surfaces and/or some degree of agglomeration of Ag(2.0)NPs that might have occurred during the deposition step.[39] However, the latter phenomenon is not likely a major contributor, as the SEM images (cf. Figure 5) reveal that the Ag(2.0)NPs on fiber surfaces are dispersed sufficiently. As demonstrated in Figure 5, the intensity of yellow color increased with increasing amount of protein adsorbed on the PP substrate, indicating increased density of Ag(2.0)NP. This finding is supported by UV−vis spectra of nonwoven surfaces, as shown in Figure 6, which show clearly an increase in intensity of the absorption peak at 404 nm with increasing protein coverage. The increased amounts of protein lead to the generation of a large fraction of positively charged groups on the surface, which are capable of anchoring Ag(2.0)NP through electrostatic interactions.

The ability of the silver nanoparticle coatings on PP nonwoven mats to provide effective antibacterial characteristics was tested by using method *a* as detailed in the Materials and

dx.doi.org/10.1021/am4011644 | *ACS Appl. Mater. Interfaces* 2013, 5, 5298−5306

Methods section. Figure 7 (left column) shows the LB agar plates with PP nonwovens before and after modification with Ag(2.0)NP to which *E. coli* was applied. No clear zone of inhibition (ZOI) was observed around the control PP and LYS-PP nonwoven mats. The presence of nanoparticles on the nonwoven surfaces inhibited the bacterial growth and exhibited a clear ZOI. The sizes of the ZOI increased with increasing amount of Ag(2.0)NP on the nonwoven surfaces. The corresponding optical images adjacent to the Petri dish demonstrate that no bacterial colonies were observed at the edge of the nonwoven. The number of cells inhibited in the ZOI was calculated for Ag(2.0)NP-treated surfaces including PP-LYS(0.44)-Ag(2.0)NP, PP-LYS(0.75)-Ag(2.0)NP and PP-LYS(1.1)-Ag(2.0)NP assuming a homogeneous distribution of cell throughout the agar slurry (the numbers in parentheses represent the corresponding fractional coverage of protein). The results are summarized in Figure 8 assuming 100%

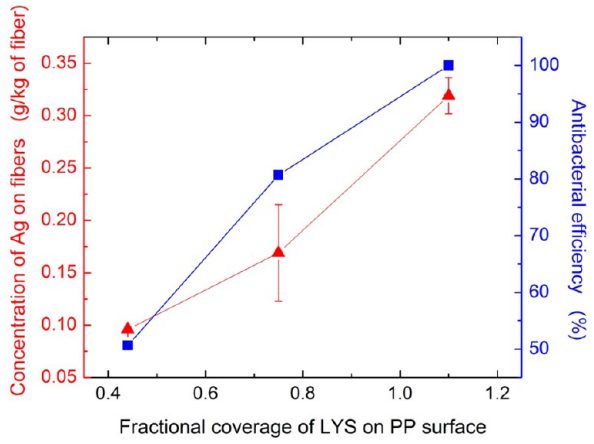

Figure 8. Antibacterial efficiency of silver nanoparticle deposited on PP surfaces calculated from test method a with increasing amount of protein on the surface. The error bars represent the standard deviation calculated from three readings.

bacterial efficiency for PP-LYS(1.1)-Ag(2.0)NP. The results indicate that the efficiency of the coating in preventing bacterial growth increases with increasing the density of the Ag(2.0)NP and thus increasing the amount of protein on the surface. Sambhy et al.[1] demonstrated that the diffusion of Ag ions from nanoparticles into the surrounding aqueous medium inhibited the bacterial growth. Parameswari et al.[40] reported an increase in the size of the ZOI with increased AgNP concentrations. Therefore, increasing the nanoparticle concentration on the fiber surface results in a higher degree of active Ag ions that leach into the surrounding aqueous medium, thus providing increased bacterial ZOI. Antibacterial testing of PP nonwoven specimens was carried out also using method *b*. Figure 7 (right column) shows bacterial colony forming units (CFU) grown on culture plates for control PP, PP-LYS, and PP-LYS-AgNP as a function of the concentration of proteins on its surface. The results obtained from antibacterial tests of the nonwoven surfaces are summarized in Table 2. The control plate was covered with a higher number density of bacterial colonies, whereas 46% bacterial reduction is observed for nonwovens treated with LYS protein. Ibrahim and co-workers[41] reported that heat-denatured LYS exhibited enhanced antibacterial activity, though its enzymatic activity is lost as compared to that in its native structure. The action of LYS against bacteria is

Table 2. Antibacterial Activity of the PP Nonwoven Surfaces before and after Modification with Proteins and Silver Nanoparticle Coating (Test Method b)

substrate[a]	% killing efficiency
control PP	
PP-LYS	46.5
PP-LYS(0.44)-Ag(2.0)NPs	99
PP-LYS(0.75)-Ag(2.0)NPs	100
PP-LYS(1.1)-Ag(2.0)NPs	100

[a]"*xx*" in PP-LYS(*xx*) represents the fractional coverage of lysozyme on PP.

due to its interaction with the bacterial membrane and its subsequent disruption. The protein-coated surfaces treated with AgNPs exhibited enhanced biocidal function. The mode of action of AgNPs on microorganisms is not well-known. Kittler et al.[42] reported that released Ag ions from citrate-capped silver nanoparticles inhibit the bacterial growth. Specifically, an approximate 2 log reduction (i.e., 99% reduction) in bacteria was observed for PP-LYS(0.44)-Ag(2.0)NP nonwoven in comparison with the control PP fabric. On the other hand, an approximately 7 log reduction (i.e., 99.99999% reduction) in bacterium was observed in PP-LYS(0.75)-Ag(2.0)NP and PP-LYS(1.1)-Ag(2.0)NP nonwoven surfaces. The results clearly demonstrate that the biocidal activity increased due to the increased concentration of nanoparticles on the surface with increased protein coverage. Hence, coatings based on proteins with adsorbed Ag(2.0)NP endow PP nonwovens with antibacterial properties.

CONCLUSIONS

A simple method was developed to form functional coatings on hydrophobic PP surfaces that impart antibacterial characteristics via the deposition of silver nanoparticles. AgNPs were prepared at different molar concentrations followed by their characterization with UV−vis spectroscopy and TEM. Negatively charged citrate-capped Ag(2.0)NPs were attached through electrostatic interactions to the positively charged functional groups present on protein primer coating PP surfaces at neutral pH conditions. The concentration of Ag(2.0)NP increased with increasing amount of protein primer on the PP surface. The deposition of Ag(2.0)NP on the surface was confirmed by UV−vis spectroscopy and SEM. Denatured LYS-coated surfaces killed *E. coli* to some extent due to their inherent antibacterial characteristics. However, the antibacterial activity of the surfaces was improved significantly with the deposition of Ag(2.0)NP to LYS-modified PP nonwovens.

A few important points remain to be answered with regard to the effectiveness of the proposed modification method under "real" conditions. Specifically, we have not tested the mechanical stability and performance of the aforementioned coatings or the effect of medium conditions, such as pH, salinity, temperature, etc. Clearly, those have to be investigated further in depth to demonstrate the universal applicability of the proposed method in "real" conditions. In addition, minimization of the cost of the coatings can be achieved by replacing lysozyme with inexpensive protein molecules that have been used in related applications. Potential candidates can be glycinin and β-conglycinin, the main proteins present in soy.[25,43,44] In fact, we have shown recently that coatings prepared from these proteins exhibit wettability and functionality that are comparable to (if not better than) lysozyme and

fibrinogen, two proteins we studied most extensively in the past.

■ ASSOCIATED CONTENT

Supporting Information

The determination of the initial amount of silver ions present in silver nitrate reduced to silver after the formation of nanoparticles. The calculations pertaining to determining the molar concentrations of nanoparticles are also provided. This material is available free of charge via the Internet at http://pubs.acs.org.

■ AUTHOR INFORMATION

Corresponding Author

*E-mail: jan_genzer@ncsu.edu. Phone: +1-919-515-2069.

Notes

The authors declare no competing financial interest.

■ ACKNOWLEDGMENTS

The authors thank the NC State University's Nonwovens Institute and Defense Threat Reduction Agency (DTRA; grant HDTRA1-10-1-0024) for supporting this work. We thank Professor Orlin Velev (NC State University) for allowing us to use the confocal microscope and Zetasizer Nano-ZS his lab. We also acknowledge Alexander Richter for helping us with determining free silver ions from silver nanoparticle solutions. Laser Imaging and Vibrational Spectroscopy Facility located in the Department of Chemistry at NC State University is acknowledged for help with FTIR spectroscopy. We also acknowledge the Chapel Hill Analytical and Nanofabrication Laboratory (CHANL) at University of North Carolina for allowing us to use SEM and TEM equipment.

■ REFERENCES

(1) Sambhy, V.; MacBride, M. M.; Peterson, B. R.; Sen, A. *J. Am. Chem. Soc.* **2006**, *128*, 9798−9808.
(2) Huang, J.; Murata, H.; Koepsel, R. R.; Russell, A. J.; Matyjaszewski, K. *Biomacromolecules* **2007**, *8*, 1396−1399.
(3) Elsabee, M. Z.; Abdou, E. S.; Nagy, K. S. A.; Eweis, M. *Carbohydr. Polym.* **2008**, *71*, 187−195.
(4) Abdelgawad, A. M.; Hudson, S. M.; Rojas, O. J. *Carbohydr. Polym.* **2013**, DOI: 10.1016/j.carbpol.2012.12.043.
(5) Yao, F.; Fu, G.-D.; Zhao, J.; Kang, E.-T.; Neoh, K. G. *J. Membr. Sci.* **2008**, *319*, 149−157.
(6) Russell, A. D. *J. Appl. Microbiol. Symp. Suppl.* **2002**, *92*, 121S−135S.
(7) Knetsch, M. L. W.; Koole, L. H. *Polymers* **2011**, *3*, 340−366.
(8) Hegstad, K.; Langsrud, S.; Lunestad, B. T.; Scheie, A. A.; Sunde, M.; Yazdankhah, S. P. *Microb. Drug Resist.* **2010**, *16*, 91−104.
(9) Morones, J. R.; Elechiguerra, J. L.; Camacho, A.; Holt, K.; Kouri, J. B.; Ramírez, J. T.; Yacaman, M. J. *Nanotechnology* **2005**, *16*, 2346−2353.
(10) Li, W.-R.; Xie, X.-B.; Shi, Q.-S.; Zeng, H.-Y.; Ou-Yang, Y.-S.; Chen, Y.-B. *Appl. Microbiol. Biotechnol.* **2010**, *85*, 1115−1122.
(11) Pal, S.; Tak, Y. K.; Song, J. M. *Appl. Environ. Microbiol.* **2007**, *73*, 1712−1720.
(12) Rai, M.; Yadav, A.; Gade, A. *Biotechnol. Adv.* **2009**, *27*, 76−83.
(13) Raffi, M.; Hussain, F.; Bhatti, T. M.; AKhter, J. I.; Hameed, A.; Hasan, M. M. *J. Mater. Sci. Tehnol.* **2008**, *24*, 192−196.
(14) Sondi, I.; Salopek-Sondi, B. *J. Colloid Interface Sci.* **2004**, *275*, 177−182.
(15) Gupta, B.; Saxena, S.; Ray, A. *J. Appl. Polym. Sci.* **2008**, *107*, 324−330.
(16) Bellel, A.; Sahli, S.; Ziari, Z.; Raynaud, P.; Segui, Y.; Escaich, D. *Surf. Coat. Technol.* **2006**, *201*, 129−135.
(17) Strobel, M.; Branch, M. C.; Ulsh, M.; Kapaun, R. S.; Kirk, S.; Lyons, C. S. *J. Adhes. Sci. Technol.* **1996**, *10*, 515−539.
(18) Zhao, J.; Shi, Q.; Luan, S.; Song, L.; Yang, H.; Shi, H.; Jin, J.; Li, X.; Yin, J.; Stagnaro, P. *J. Membr. Sci.* **2011**, *369*, 5−12.
(19) Piletsky, S. A.; Matuschewski, H.; Schedler, U.; Piletska, E. V.; Thiele, T. A.; Ulbricht, M. *Analysis* **2000**, 3092−3098.
(20) Krause, B.; Voigt, D.; Häußler, L.; Auhl, D.; Münstedt, H. *J. Appl. Polym. Sci.* **2006**, *100*, 2770−2780.
(21) Mao, C.; Zhang, C.; Yongzhi, Q.; Aiping, Z.; Shen, J.; Lin, S. *Appl. Surf. Sci.* **2004**, *228*, 26−33.
(22) Abdou, E. S.; Elkholy, S. S.; Elsabee, M. Z.; Mohamed, E. *J. Appl. Polym. Sci.* **2008**, *108*, 2290−2296.
(23) Goli, K. K.; Rojas, O. J.; Genzer, J. *Biomacromolecules* **2012**, *13*, 3769−3779.
(24) Goli, K. K.; Rojas, O. J.; Ozçam, A. E.; Genzer, J. *Biomacromolecules* **2012**, *13*, 1371−1382.
(25) Salas, C.; Rojas, O. J.; Lucia, L. A.; Hubbe, M. A; Genzer, J. *Biomacromolecules* **2012**, *13*, 387−96.
(26) Salas, C.; Rojas, O. J.; Lucia, L. A.; Hubbe, M. A.; Genzer, J. *ACS Appl. Mater. Interfaces* **2013**, *5*, 199−206.
(27) Murphy, C. J.; Jana, N. R. *Adv. Mater.* **2002**, *14*, 80−82.
(28) Jana, N. R.; Gearheart, L.; Murphy, C. J. *Chem. Commun.* **2001**, 617−618.
(29) Paula, M. M. S.; Costa, C. S.; Baldin, M. C.; Scaini, G.; Rezin, G. T.; Segala, K.; Andrade, V. M.; Franco, C. V.; L, S. E. *J. Braz. Chem. Soc.* **2009**, *20*, 1556−1560.
(30) Praus, P.; Turicová, M.; Klementová. *J. Braz. Chem. Soc.* **2009**, *20*, 1351−1357.
(31) Munro, C. H.; Smith, W. E.; Garner, M.; Clarkson, J.; White, P. C. *Langmuir* **1995**, *11*, 3712−3720.
(32) Dong, X.; Ji, X.; Jing, J.; Li, M.; Li, J.; Yang, W. *J. Phys. Chem. C* **2010**, *114*, 2070−2074.
(33) Lu, Y.-C.; Chou, K.-S. *J. Chin. Inst. Chem. Eng.* **2008**, *39*, 673−678.
(34) Turkevich, J. *Gold Bull.* **1985**, *18*, 86−91.
(35) Cumberland, S. A.; Lead, J. R. *J. Chromatogr., A* **2009**, *1216*, 9099−9105.
(36) Farris, S.; Song, J.; Hunag, Q. *J. Agric. Food Chem.* **2010**, *58*, 998−1003.
(37) Kong, J.; Yu, S. *Acta Biochim. Biophys. Sin.* **2007**, *39*, 549−559.
(38) Mandal, S.; Gole, A.; Lala, N.; Gonnade, R.; Ganvir, V.; Sastry, M. *Langmuir* **2001**, *17*, 6262−6268.
(39) Dubas, S. T.; Wacharanad, S.; Potiyaraj, P. *Colloids Surf., A* **2011**, *380*, 25−28.
(40) Parameswari, E.; Udayasoorian, C.; Sebastian, S. P.; Jayabalakrishnan, R. M. *Int. Res. J. Biotechnol.* **2010**, *1*, 44−49.
(41) Ibrahim, H. R.; Higashiguchi, S.; Koketsu, M.; Juneja, L. R.; Kim, M.; Yamamoto, T.; Sugimoto, Y.; Aoki, T. *J. Agric. Food Chem.* **1996**, *44*, 3799−3806.
(42) Kittler, S.; Greulich, C.; Diendorf, J.; Köller, M.; Epple, M. *Chem. Mater.* **2010**, *22*, 4548−4554.
(43) Salas, C.; Rojas, O. J.; Lucia, L. A.; Hubbe, M. A.; Genzer, J. *ACS Appl. Mater. Interfaces* **2013**, *5*, 199−206.
(44) Salas, C.; Genzer, J.; Lucia, L. A.; Hubbe, M. A.; Rojas, O. J. *ACS Appl. Mater. Interfaces* **2013**, submitted for publication.